 doi:10.20944/preprints202207.0284.v1

Article

Orbital and Spin Dynamics of Electron's States Transition in Hydrogen Atom Driven by Electric Field

Ciann-Dong Yang [1] and Shiang-Yi Han [2,*]

[1] Department of Aeronautics and Astronautics, National Cheng Kung University, Tainan, Taiwan, R.O.C.; cdyang@mail.ncku.edu.tw
[2] Department of Applied Physics, National Kaohsiung University, Kaohsiung, Taiwan, R.O.C.; syhan.taiwan@gmail.com
* Correspondence: syhan.taiwan@gmail.com

Abstract: State transition in the multiple-levels system has the great potential applications in the quantum technology. In this article we employ a deterministic approach in complex space to analyze the dynamics of the 1s-2p electron transition in the hydrogen atom. The electron's spin motion is embodied in the framework of quantum Hamilton mechanics that allows us to examine the transition dynamics more precisely. The transition is driven by an oscillating electric field in the z −direction. The electron's transition process can be visualized by monitoring its motion in the complex space. The quantum potential and the total energy proposed in this paper provide new indices to observe the dynamic changes of electrons in the transition process.

Keywords: two-level transition; electron dynamics; spin dynamics; spin angular momentum perturbation

1. Introduction

The multiple-level system has widely applications in different scientific fields, such as the atomic clock, information storage, and quantum computing, and so on [1-5]. Quantum transitions in multiple-level states have been studied in different systems with some studies focusing on the excitation resources and the theoretical methods [6-15]. The hydrogen atom is one of the basic system considered in the level-energy transition problem. In the trajectory interpretation of quantum mechanics, Bohmian mechanics is one of the most used theories to model the quantum systems. However, Bohmian mechanics is developed based on the Schrödinger equation which has no spin counterpart. Therefore, the original Bohm's guidance law is not adapted to the system with spin particle. To include the spin effect, a modified guidance law was proposed [16] to study spin-dependent Bohm trajectories associated with an electronic transition in hydrogen. This modified guidance laws provides a trajectory-based platform for researchers to study the electron's energy-level transitions [17-21].

In addition to the modified Bohmian guidance law, many studies deal with the complex-extended quantum systems, such as complex energy [22,23], complex time [24-26], complex space [27-29], complex photonic lattices [30], and so on. After the weak value method has been proposed, the eigenvalues of the measured quantity are not constrained to the real number [31-34]. Corresponding to the experimental concept, the weak measurement is able to observe a quantum system in a minimum interfering condition so that it allows scientists to acquire the classical-counterpart physical quantities of the quantum system with the complex eigenvalues. The quantum trajectory has been observed in different systems by means of the weak measurement [35-42]. The features of the non-Hermitian system and parity time have been detected by using the weak value method [43-46]. In 2021, two experiments revealed that the imaginary number in quantum mechanics has the physical meaning in reality [47,48]. According to these experimental results, the complex number appeared in the Schrödinger equation is not merely a mathematical tool but has an actual physical meaning [49,50].

Quantum Hamilton mechanics (QHM) is one of the trajectory interpretation of quantum mechanics. It is established on the foundation of the complex-space structure within which all physics quantities are complex-valued [51]. The quantum operators, quantization rules, uncertainty principle, correspondence principle, quantum probability, spin, and all other fundamental properties of quantum mechanics can have their corresponding trajectory-based descriptions underlying the framework of QHM in the complex domain [52-55]. It was found that the spin motion of the electron in the hydrogen atom is independent of the wave function, and is determined solely by the geometrical property of the complex- space structure [56,57]. The combined orbital and spin motion in the hydrogen atom can therefore be precisely described in detail under the framework of QHM. It provides us the most finery model to discuss the electron's transition in the hydrogen energy levels.

In this article, we apply an oscillating electric field to the hydrogen electron to analyze its transition dynamics by means of QHM. The transition trajectory, the time evolution of the electron's total energy, and the time responses of the transition process are presented in addition to the occupation probability, which is the only information that quantum mechanics can provide. The paper is organized as follows. QHM as the main framework will be briefly introduced in Section 2, where the dynamics and the trajectories of the hydrogen electron in the complex spherical coordinate are analyzed to reveal the forces and the quantum potential acting on the electron. Section 3 will derive the spin dynamics from the Schrödinger equation and the wavefunction-independent feature of the spin dynamics will be demonstrated by means of the hydrogen electron in the ground state. With the established orbital and spin dynamics, the 1s-2p transition dynamics in the hydrogen atom will be considered in Section 4. Conclusions and discussions are given in Section 5.

2. Quantum Hamilton Mechanics

2.1 Quantum Motion in Arbitrary Force Field

In this section we will introduce the quantum Hamilton mechanics (QHM) to analyze the quantum motion under the action of the potential field $V(r,\theta,\phi)$ in the complex spherical coordinates $(r,\theta,\phi)\in\mathbb{C}^3$. The quantum Hamiltonian [56] of the particle in the quantum state $\psi(r,\theta,\phi)$ is described by

$$H=\frac{1}{2m}\left[p_r^2+\frac{\hbar}{i}\left(\frac{2}{r}p_r+\frac{\hbar}{i}\frac{\partial^2\ln\psi}{\partial r^2}\right)\right]+\frac{1}{2mr^2}\left[p_\theta^2+\frac{\hbar}{i}\left(p_\theta\cot\theta+\frac{\hbar}{i}\frac{\partial^2\ln\psi}{\partial\theta^2}\right)+\frac{1}{\sin^2\theta}\left(p_\phi^2-\hbar^2\frac{\partial^2\ln\psi}{\partial\phi^2}\right)\right]+V(r,\theta,\phi), \tag{2.1}$$

where the canonical momentum $(p_r,p_\theta,p_\phi)\in\mathbb{C}^3$ is related to ψ via the following relations,

$$p_r=\frac{\hbar}{i}\frac{\partial\ln\psi}{\partial r}=\frac{\partial S}{\partial r},\qquad p_\theta=\frac{\hbar}{i}\frac{\partial\ln\psi}{\partial\theta}=\frac{\partial S}{\partial\theta},\quad p_\phi=\frac{\hbar}{i}\frac{\partial\ln\psi}{\partial\phi}=\frac{\partial S}{\partial\phi}. \tag{2.2}$$

The complex action function S is related to ψ via $S=-i\hbar\ln\psi$. If Eqs. (2.2) is substituted into Eq. (2.1), we recover the Schrödinger equation,

$$\frac{\hbar^2}{2m}\nabla^2\psi+(H-V)\psi=0, \tag{2.3}$$

where $H=E$ is the conserved total energy of the particle. The quantum Hamiltonian (2.1) can be used to derive the Hamilton equations of motion of the particle as follows,

$$\dot{r}=\frac{\partial H}{\partial p_r}=\frac{\hbar}{im}\frac{1}{\psi}\frac{\partial\psi}{\partial r}+\frac{\hbar}{i}\frac{1}{mr}, \tag{2.4a}$$

$$\dot{\theta}=\frac{\partial H}{\partial p_\theta}=\frac{\hbar}{mri}\frac{1}{\psi}\frac{\partial\psi}{\partial\theta}+\frac{\hbar}{i}\frac{\cot\theta}{2mr^2}, \tag{2.4b}$$

$$\dot{\phi}=\frac{\partial H}{\partial p_\phi}=\frac{1}{mr\sin^2\phi}\frac{\hbar}{i}\frac{1}{\psi}\frac{\partial\psi}{\partial\phi}. \tag{2.4c}$$

Preprints (www.preprints.org) | NOT PEER-REVIEWED | Posted: 19 July 2022 doi:10.20944/preprints202207.0284.v1

In terms of $(\dot{r},\dot{\theta},\dot{\phi})$, the quantum Hamiltonian H can be rewritten in a classical analog form:

$$H=\frac{m}{2}\left[\dot{r}^2+\left(r\dot{\theta}\right)^2+\left(r\dot{\phi}\sin\theta\right)^2\right]+V_{\text{Total}}, \tag{2.5}$$

in which the terms in the bracket constitute the classical counterpart of the kinetic energy, and $V_{\text{Total}}=Q+V$ represents the total potential which contains the quantum potential Q and the external potential $V(r,\theta,\phi)$:

$$V_{\text{Total}}=\left\{\frac{\hbar^2}{8mr^2}(4+\cot^2\theta)-\frac{\hbar^2}{2m}\left[\frac{\partial^2\ln\psi}{\partial r^2}+\frac{1}{r^2}\frac{\partial^2\ln\psi}{\partial\theta^2}+\frac{1}{r^2\sin^2\theta}\frac{\partial^2\ln\psi}{\partial\phi^2}\right]\right\}+V(r,\theta,\phi). \tag{2.6}$$

In Bohr's atomic model, the dominant potential is the Coulomb potential $V(r)$ which attracts the electron to the nucleus so that the electron eventually will fall on the nucleus; however, it never happens in reality. Eq. (2.6) proposes an explanation of how atom can keep balanced between the quantum potential Q and the Coulomb potential $V(r)$. The quantum potential Q, which is responsible for all the quantum effects, can be recognized as the potential barrier, which stops the electron crashing on the nucleus. The quantum potential Q is related to the wavefunction $\psi(r,\theta,\phi)$ as

$$V_{\text{Total}}=V+Q=\frac{\hbar^2}{2m}\frac{(\nabla\psi)^2}{\psi\psi^*}. \tag{2.7}$$

In fact, the quantum potential determines the spatial distribution of the electron in the atomic model for the reason that it is inversely proportional to the probability density function $\psi\psi^*$ as shown in Eq. (2.7).

2.2 Orbital Dynamics of Electron in Hydrogen Atom

The central-force field in the hydrogen atom is specified by the Coulomb potential:

$$V=V(r)=\frac{-e^2}{4\pi\varepsilon_0 r}, \tag{2.8}$$

where r is the distance between the electron and the nucleus. The solution of the Schrödinger equation (2.3) with $V=V(r)$ is separable as

$$\psi_{nlm_l}(r,\theta,\phi)=CR_{nl}(r)\Theta_{lm_l}(\theta)\Phi_{m_l}(\phi), \tag{2.9}$$

where l and m_l denote the orbital quantum number and the magnetic quantum number, respectively. The three separated functions are related to the Laguerre polynomial $L_{n-l-1}^{2l+1}(r)$, associated Legendre polynomial $P_l^{m_l}(\cos\theta)$, and the exponential function as follows:

$$R_{nl}(r)=(2r/n)^l e^{-r/n}L_{n-l-1}^{2l+1}(2r/n), \tag{2.10a}$$
$$\Theta_{lm_l}(\theta)=P_l^{m_l}(\cos\theta),\quad l=0,1,2,\cdots,n-1, \tag{2.10b}$$
$$\Phi_{m_l}(\phi)=e^{im_l\phi},\qquad m_l=0,\pm1,\pm2,\cdots,\pm l. \tag{2.10c}$$

The eigenenergy E_n is related to the principle quantum number n as

$$E_n=-\left(\frac{\hbar^2}{2ma_0}\right)\frac{1}{n^2}, \tag{2.11}$$

where a_0 is the Bohr radius. By inserting the wavefunction (2.9) into Eqs. (2.4), we obtain the equations of motion for the electron moving in the eigenstate:

$$\frac{d\rho}{d\tau}=\frac{2}{i}\frac{d}{d\rho}\ln\left(\rho R_{nl}(\rho)\right), \tag{2.12a}$$
$$\frac{dz_\theta}{d\tau}=\frac{1}{i\rho^2}\left[2(1-z_\theta^2)\frac{d}{dz_\theta}\ln\left(\Theta_{lm_l}(z_\theta)-z_\theta\right)\right],\quad z_\theta=\cos\theta, \tag{2.12b}$$
$$\frac{d\phi}{d\tau}=\frac{2m_l}{\rho^2\left(1-z_\theta^2\right)}, \tag{2.12c}$$

where the dimensionless radius $\rho=r/a_0$ and the dimensionless time $\tau=t\hbar/(2ma_0^2)$ are applied.

The total potential that the electron encounters in the hydrogen atom can be obtained by inserting the wave function (2.9) to Eq. (2.6),

$$\bar{V}_{nl\ \ l}=\bar{V}+\bar{Q}=-\frac{2}{\rho}+\left[\frac{(4+\cot^2\theta)}{4\rho^2}-\frac{d^2\ln R_{nl}(\rho)}{d\rho^2}-\frac{1}{\rho^2}\frac{d^2\ln\Theta_{lm_l}(\theta)}{d\theta^2}\right], \tag{2.13}$$

 doi:10.20944/preprints202207.0284.v1

where the terms with bar denote the dimensionless form. The terms within the bracket constitute the quantum potential $\bar{Q}$ and cause the formation of the shell structures in the hydrogen atom. The derivatives of V_{nlm_l} with respect to ρ, θ, and ϕ give the total forces acting on the electron:

$$\bar{f}^{\rho}_{nlm_l} = -\frac{2}{\rho^2} + \frac{1}{2\rho^3}(4 + \cot^2\theta) - \frac{d^3 \ln R_{nl}(\rho)}{d\rho^3} - \frac{2}{\rho^2}\frac{d^2 \ln \Theta_{lm_l}(\theta)}{d\theta^2}, \tag{2.14a}$$

$$\bar{f}^{\theta}_{nlm_l} = \frac{1}{\rho^2}\frac{d^3 \ln \Theta_{lm_l}(\theta)}{d\theta^3} + \frac{1}{2\rho^2}\frac{\cos\theta}{\sin^3\theta}, \tag{2.14b}$$

$$\bar{f}^{\phi}_{nlm_l} = \frac{1}{\rho^2 \sin^2\theta}\frac{d^3 \ln \Phi_{m_l}(\phi)}{d\phi^3} = 0. \tag{2.14c}$$

One can picturize how the electron moves in a specific eigenstate by analyzing the total forces acting on it. Taking the 1s state with $(n, l, m_l) = (1,0,0)$ as an example, the total force can be acquired from Eqs. (2.14) with the ground-state wavefunction, $R_{10}(\rho) = e^{-\rho}$ and $\Theta_{00}(\theta) = \Phi_0(\phi) = 1$,

$$\bar{f}^{\rho}_{100} = -\frac{2}{\rho^2} + \frac{1}{2\rho^3}(4 + \cot^2\theta), \quad \bar{f}^{\theta}_{100} = \frac{1}{2\rho^2}\frac{\cos\theta}{\sin^3\theta}, \quad f^{\phi}_{100} = 0. \tag{2.15}$$

The position satisfying $\bar{f}^{\rho}_{100} = \bar{f}^{\theta}_{100} = \bar{f}^{\phi}_{100} = 0$ is called the equilibrium position and is found as

$$\rho_{\mathrm{eq}} = 1, \quad \theta_{\mathrm{eq}} = \pi/2. \tag{2.16}$$

The electron has the tendency to stay at the equilibrium position since it is the most stable place in a dynamic sense. The tendency of being at $\rho_{\mathrm{eq}} = 1$ (or equivalently, $r_{\mathrm{eq}} = a_0$), is compatible with the probability distribution $P_{10}(\rho) = 4\pi\rho^2 e^{-2\rho}$, which achieves its maximum at the Bohr radius a_0, i.e., at the equilibrium position $\rho_{\mathrm{eq}} = 1$. The correspondence between the particle dynamic and the wave probability is one of the significant features of the hydrogen electron revealed by QHM. Another feature shows that the electron mostly lays on the $x - y$ plane since $\theta_{\mathrm{eq}} = \pi/2$. The electron cloud may have the brightest (intense) part focusing on a ring with radius a_0 on the $x - y$ plane if combining the two features together. The radial force at $\theta_{\mathrm{eq}} = \pi/2$ is

$$\bar{f}^{\rho}_{100}(\rho, \pi/2) = \bar{f}^{\rho}_{V}(\rho) + \bar{f}^{\rho}_{Q}(\rho) = -\frac{2}{\rho^2} + \frac{2}{\rho^3}, \tag{2.17}$$

where the subscripts V and Q denote the Coulomb force and the quantum force, respectively. Obviously, the quantum force is much greater than the Coulomb force when $\rho < 1$, which means that the quantum force forbids the electron crashing on the nucleus. This is the third remarkable feature of the hydrogen electron revealed by QHM.

The motion of the electron in the ground state can be obtained from Eqs. (2.12):

$$\frac{d\rho}{d\tau} = \frac{2}{i}\frac{1-\rho}{\rho}, \quad \frac{dz_\theta}{d\tau} = \frac{z_\theta}{i\rho^2}, \quad \frac{d\phi}{d\tau} = 0. \tag{2.18}$$

Fig. 1a displays some complex trajectories projected on the real $x - z$ plane ($\phi = 0$), which are solved from Eq. (2.18) with different initial positions. The electron is moving oscillatory with the same period as can be observed in Fig. 1b. In particular, the electron almost stays at the equilibrium radius $\rho_{\mathrm{eq}} = 1$ if its initial position is on it, as Fig. 1c shows. It is clear to see from Fig. 1d that the oscillating trajectory has the period of 2π. The periodic trajectory is the fourth feature of the hydrogen electron, which represents the energy conversation. Please note that the electron's motion can happen in any value of ϕ between 0 and 2π since the wavefunction is spherically symmetric and $\dot{\phi} = 0$.

Preprints (www.preprints.org) | NOT PEER-REVIEWED | Posted: 19 July 2022 doi:10.20944/preprints202207.0284.v1

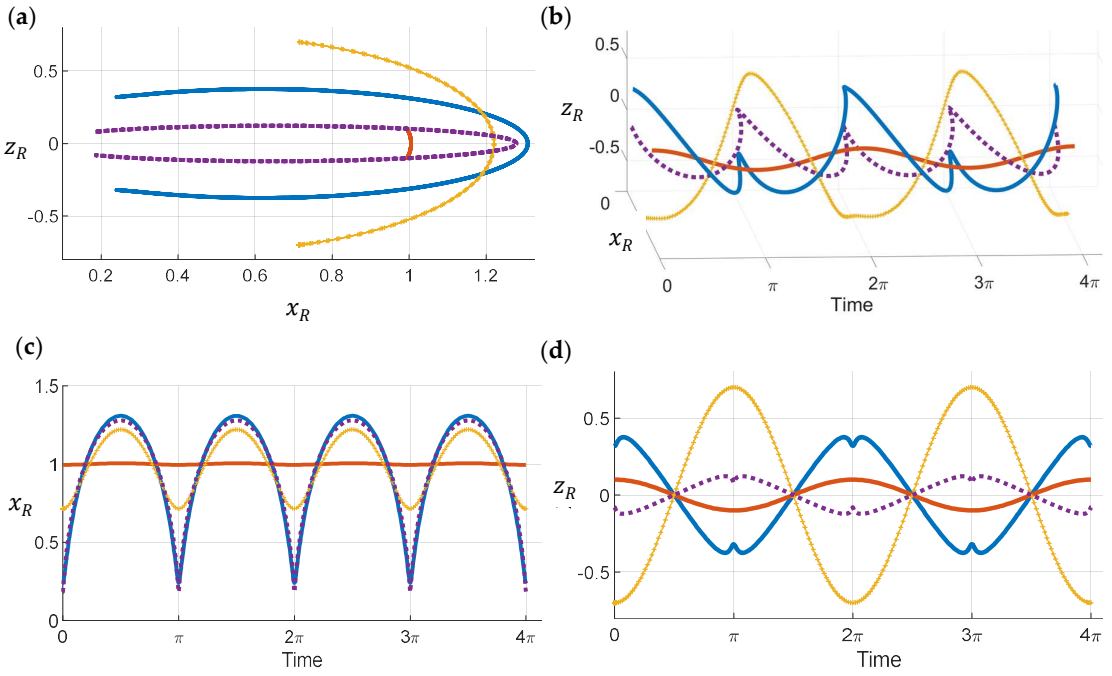

Figure 1. (**a**) The complex trajectories in the real $x-z$ plane starting from initial positions: $(\rho(0), z_\theta(0)) = (0.4, 0.8)$, $(1, 0.1)$, $(1, -0.7)$, and $(0.2, -0.4)$, are displayed, respectively, by solid-blue line, solid-red line, dashed-purple line, and solid-yellow line. (**b**) The four trajectories with different initial positions have the same period of 2π. (**c**) The time responses of $x_R = \mathrm{Re}(\rho\sin\theta)$ oscillate with respect to its equilibrium position $x_R = 1$. (**d**) The time responses of $z_R = \mathrm{Re}(\rho\cos\theta)$ oscillate with respect to its equilibrium position $z_R = 0$.

Fig. 2a illustrates the complex trajectories of the electron in the $2s$ state projected on the real $x-z$ plane. The equations of motion for the $2s$ state read,

$$\frac{d\rho}{d\tau} = i\frac{\rho^2 - 6\rho + 4}{\rho(\rho - 2)}, \quad \frac{dz_\theta}{d\tau} = \frac{z_\theta}{i\rho^2}, \quad \frac{d\phi}{d\tau} = 0. \tag{2.19}$$

We notice that there are two equilibrium positions in the radial direction and one in the azimuthal direction,

$$\rho_{\mathrm{eq}} = 3 \pm \sqrt{5}, \quad \theta_{\mathrm{eq}} = \pi/2. \tag{2.20}$$

Two equilibrium positions in the radial direction reflect that there are two shell structures of the electron cloud (probability distribution) separated by the boundary $\rho = 2$. The electron is allowed to move either in the first shell $0 < \rho < 2$ or the second shell $\rho > 2$. The trajectories illustrated in Fig. 2a can be divided into two groups. The inner group corresponds to the motions in the first shell and the outer group corresponds to the motion in the second shell. The shell structure is formed by the spatial distribution of the total potential,

$$\bar{V}_{200} = \bar{V} + \bar{Q} = -\frac{2}{\rho} + \left[-\frac{2}{(2-\rho)^3} + \frac{1}{2\rho^2}(4 + \cot^2\theta)\right]. \tag{2.21}$$

In fact, the quantum potential contributes the most part of the shell structure as represented by Eq. (2.21). Fig. 2b illustrates the total potential in the radial direction. The two equilibrium positions $\rho_{\mathrm{eq}} = 3 \pm \sqrt{5}$ are at the lowest points in the two shells of $\bar{V}_{200}$.

 doi:10.20944/preprints202207.0284.v1

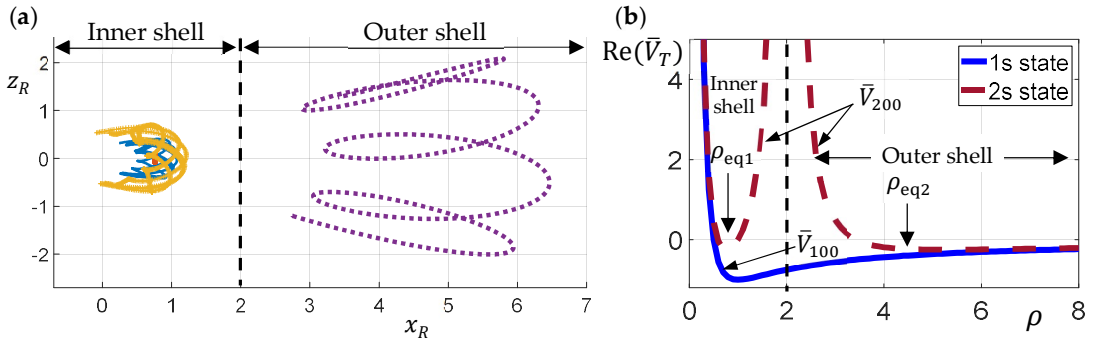

Figure 2. (**a**) The Electron's trajectory in the real $x-z$ plane with initial positions $(\rho(0), z_\theta(0)) = (0.4,0.8)$, $(3-\sqrt{5}, 0.1)$, $(1,-0.7)$, and $(3,-0.4)$ are represented, respectively, by solid-blue line, solid-red line, solid-yellow line, and dashed-purple line. (**b**) The real-part total potential in the 1s state and 2s state, $\bar{V}_{100}$ and $\bar{V}_{200}$, has the equilibrium radius at $\rho_{\mathrm{eq}} = 1$ and $\rho_{\mathrm{eq}} = 3 \pm \sqrt{5}$, respectively.

3. Spin Dynamics of Electron in Hydrogen Atom

3.1 Spin Dynamics in Complex Space

The eigenstate of the hydrogen electron with zero orbital angular momentum $(l = 0)$ is spherically symmetric and decays more or less exponentially with increasing distance from the origin. It is noted that the electron in the state with zero orbital angular momentum, such as $1s$ or $2s$ state, still has nonzero probability distribution in the azimuthal direction. However, the motion with zero orbital angular momentum could happen only if the electron is oscillating along the straight line connecting the electron and the nucleus in a classical sense. In QHM this contrary observation between the quantum perspective and classical perspective about the zero angular momentum can be explained. From Eq. (2.18) and Eq. (2.19) we can see that the electron is not only moving in the radial direction but also in the azimuthal direction in both 1s and 2s states. This azimuthal motion is caused by a special term $(4+\cot^2\theta)/4\rho^2$ in the total potential, which in turn generates a force component $\cos\theta/2\rho^2\sin^3\theta$ in the θ-direction, as can be seen in Eq. (2.14b). Thus, the electron moves in the azimuthal direction even if the orbital angular momentum is zero. This is the most significant feature of the electron and is recognized as the spin motion

The combined orbital and spin motion of the electron is described by (2.4b)

$$mr^2\dot{\theta} = p_\theta + p_s = \frac{\hbar}{i}\frac{d\ln\Theta_{lm_l}(\theta)}{d\theta} + \frac{\hbar}{2i}\cot\theta, \tag{3.1}$$

where p_θ and p_s denote the orbital angular momentum and the spin angular momentum, respectively. The spin angular momentum p_s is responsible for the angular motion when the orbital angular momentum p_θ is zero:

$$mr^2\dot{\theta} = p_s = \frac{\hbar}{2i}\cot\theta. \tag{3.2}$$

The evaluation of the mean value of the spin angular momentum p_s at the Bohr radius $(\rho = 1)$ gives the following results:

$$\langle mr^2\frac{d\theta}{dt}\rangle = \frac{\hbar}{2}\langle\rho^2\frac{d\theta}{d\tau}\rangle = \pm\frac{\hbar}{2}, \tag{3.3}$$

where the positive and negative signs represent the spin up and spin down, respectively. Spin is a unique quantum feature that has no classical counterpart. However, in the framework of QHM, spin motion can be demonstrated in a classical manner. What makes QHM so special that it can describe explicitly the electron's spin motion? The answer is hidden

 doi:10.20944/preprints202207.0284.v1

in the extension of the space dimension. The spin angular momentum can never be shown by Eq. (3.3) if the extension to complex space is not considered.

Eq. (3.3) can be proved by considering the electron in the ground state [57]. Recall that the radial force acting on the electron in the ground state is given by Eq. (2.15):

$$\bar{f}_{100}^{\rho} = -\frac{2}{\rho^2} + \frac{1}{2\rho^3}(4 + \cot^2\theta) = \bar{f}_C^{\rho} + \bar{f}_Q^{\rho}, \tag{3.4}$$

which is composed of the attractive Coulomb force $\bar{f}_C^{\rho}$ and repulsive quantum force $\bar{f}_Q^{\rho}$. There is no radial force acting on the electron when it is at the equilibrium position $\rho_{\text{eq}} = 1,\ \theta_{\text{eq}} = \pi/2$ according to Eq. (3.4). When the electron deviates from the equilibrium position, $\bar{f}_C^{\rho}$ and $\bar{f}_Q^{\rho}$ become unequal,

$$\bar{f}_C^{\rho} < \bar{f}_Q^{\rho}, \quad \rho < 1, \tag{3.5a}$$

$$\bar{f}_C^{\rho} > \bar{f}_Q^{\rho}, \quad \rho > 1. \tag{3.5b}$$

In either case, there is a force driving the electron to return to the equilibrium position. Similarly, the total tangential force $\bar{f}_{100}^{\theta} = 0$ at $\theta_{\text{eq}} = \pi/2$ can be obtained according to Eq. (2.15). Therefore, the electron has a stable oscillation motion around the equilibrium point, which can be described mathematically by

$$\rho(\tau) = 1 + \text{Lambert}W(e^{2i\tau + c_0}), \tag{3.6a}$$

$$\cos\big(\theta(\tau)\big) = \frac{c_1 e^{i\tau + c_0}}{\sqrt{e^{\text{Lambert}W(e^{2i\tau+c_0})} + e^{2i\tau+c_0}}}, \tag{3.6b}$$

where the special function $y = \text{Lambert}W(x)$ is defined as the solution of equation $ye^y = x$. The oscillatory motion has the zero-mean property,

$$\langle \frac{d\rho}{d\tau} \rangle = \langle \frac{d\theta}{d\tau} \rangle = 0, \tag{3.7}$$

which leads to the zero angular momentum,

$$\langle mr^2 \frac{d\theta}{dt} \rangle = \frac{\hbar}{2} \langle \rho^2 \frac{d\theta}{d\tau} \rangle = 0. \tag{3.8}$$

This significant result reveals that the electron has no spin motion in the neighborhood of the equilibrium position $(\rho_{\text{eq}}, \theta_{\text{eq}})$ in the $l = 0$ state. The electron in such a situation is said to be in a spinless mode. Fig. 3a illustrates the electron's motion in the complex θ −plane. The zero-mean property of $d\theta/d\tau$ in spinless mode can be observed in Fig. 3b.

How the electron could have no spin motion if spin is its intrinsic feature? If it is the fact, then how could scientists never observe the spinless electron? The answer is that there is only a small region in the complex space, within which the electron has no spin motion. The spinless motion only happens in the neighborhood of the equilibrium position, $(\theta_R, \theta_I) = (\pi/2\,, 0)$. As shown in Fig. 3a, the equilibrium position $(\theta_R, \theta_I) = (\pi/2\,, 0)$ is a center surrounded by closed phase-lane trajectories. Even the circling motion with greater radius has the faster $\dot{\theta}_R$ as pointed by Fig. 3b, the average value of $\dot{\theta}_R$ is still zero around the closed trajectories. When the initial position $(\theta_R(0), \theta_I(0))$ is not in the neighborhood of the equilibrium position, for example, $(\theta_R(0), \theta_I(0)) = (0, 0.5)$, the electron's motion in the complex θ −plane does not follow a closed path but a oscillatory open trajectory forwarding to the negative θ_R direction, as the dotted green line illustrates in Fig. 3c. This oscillatory trajectory has a nonzero mean value of $d\theta/d\tau$ equal to -1, as Fig. 3d shows. This oscillating motion in the complex θ −plane leads to the following result:

$$\langle mr^2 \frac{d\theta}{dt} \rangle = \frac{\hbar}{2} \langle \rho^2 \frac{d\theta}{d\tau} \rangle = -\frac{\hbar}{2}, \tag{3.9}$$

which can be recognized as the spin angular momentum with negative sign, i.e., the spin-down angular momentum.

Similarly, the angular momentum of the spin-up motion can be observed in the lower half region of the complex θ −plane. For instance, the oscillating trajectory forwarding to the positive θ_R direction is observed with $(\theta_R(0), \theta_I(0)) = (0, -0.5)$, as the dotted green line displays in Fig. 3e. The corresponding average value of $d\theta/d\tau$ is equal to 1, which is displayed in Fig. 3f. Hence, we have

$$\langle mr^2 \frac{d\theta}{dt} \rangle = \frac{\hbar}{2} \langle \rho^2 \frac{d\theta}{d\tau} \rangle = \frac{\hbar}{2}, \tag{3.10}$$

Preprints (www.preprints.org) | NOT PEER-REVIEWED | Posted: 19 July 2022 doi:10.20944/preprints202207.0284.v1

which is the spin-up angular momentum.

The three modes of the electron's spin dynamics introduced above can be further analyzed by solving Eq. (2.18) for $\theta(\tau)$ at $\rho = \rho_{\text{eq}} = 1$:

$$\cos\theta(\tau) = (\cos\theta_0)e^{i\tau}, \quad \theta_0 \in \mathbb{C}, \tag{3.11}$$

which has the property,

$$|\cos\theta(\tau)| = |\cos\theta_0| = \text{constant}. \tag{3.12}$$

With the substitution $\theta = \theta_R + i\theta_I$ into solution (3.12), the trajectory in the complex $\theta-$plane can be obtained as follows,

$$\cosh^2\theta_I = |\cos\theta_0|^2 + 1 - \cos^2\theta_R \geq 1. \tag{3.13}$$

It can be seen that $|\cos\theta_0| = 1$ is the bifurcation curve in that the θ_R dynamics is bounded if $|\cos\theta_0| < 1$, and is unbounded if $|\cos\theta_0| \geq 1$. Hence, the trajectory corresponds to the three spin modes can be divided by the boundary curve:

$$|\cos\theta| = 1 \leftrightarrow |\sinh\theta_I| = |\sin\theta_R| \tag{3.14}$$

Along the boundary curve (3.14), the three spin regions can be defined as follows,

$$\text{Spin down region } S_\downarrow \triangleq \{(\theta_R, \theta_I)|\sinh\theta_I \geq |\sin\theta_R|\}, \tag{3.15a}$$

$$\text{Spinless reqion } S_0 \triangleq \{(\theta_R, \theta_I)|\sinh\theta_I < |\sin\theta_R|\}, \tag{3.15b}$$

$$\text{Spin up region } S_\uparrow \triangleq \{(\theta_R, \theta_I)|\sinh\theta_I \leq -|\sin\theta_R|\}. \tag{3.15c}$$

The mean value of $d\theta/d\tau$ corresponding to the three spin modes are acquired by integrating $d\theta/d\tau$ to one period:

$$\langle\frac{d\theta}{d\tau}\rangle = \frac{1}{2\pi}\int_0^{2\pi}\left(\frac{d\theta}{d\tau}\right)d\tau = \begin{cases} -1, & \forall\theta_R(\tau) \in S_\downarrow \\ 0, & \forall\theta_R(\tau) \in S_0, \\ 1, & \forall\theta_R(\tau) \in S_\uparrow \end{cases} \tag{3.16}$$

and corresponding angular momentum read

$$\langle mr^2\frac{d\theta}{dt}\rangle = \frac{\hbar}{2}\langle\rho^2\frac{d\theta}{d\tau}\rangle = \begin{cases} -\hbar/2, & \forall\theta_R(\tau) \in S_\downarrow \\ 0, & \forall\theta_R(\tau) \in S_0. \\ \hbar/2, & \forall\theta_R(\tau) \in S_\uparrow \end{cases} \tag{3.17}$$

It can be shown that $\langle d\theta_I/d\tau\rangle$ is zero for all the three spin modes, and the nonzero mean value of $d\theta/d\tau$ is solely contributed by $d\theta_R/d\tau$, i.e., $\langle d\theta/d\tau\rangle = \langle d\theta_R/d\tau\rangle$. In general, the above analysis of electron's spin dynamics is valid for all states with $l = m_l = 0$. The electron is found to have no spin in a very small region in the complex space, which is around the equilibrium point. Out of the nearby region of the equilibrium point, the electron has the spin motion. The spin motions can be distinguished as spin up and spin down according to whether the trajectory in the complex $\theta-$plane is forwarding to the positive or negative θ_R direction. The nonzero mean value of $d\theta/d\tau$ leads to the spin angular momentum $\pm\hbar/2$.

It has to be pointed out that the commonly known spin angular momentum $\pm\hbar/2$ is referred to the mean value $\langle mr^2 d\theta/dt\rangle$, but not to the instantaneous value of $mr^2 d\theta/dt$. Indeed, $d\theta/d\tau$ or $d\theta_R/d\tau$ is oscillating with time, as illustrated in Fig. 3d and Fig. 3f. The oscillation period of $d\theta_R/d\tau$ is 2π whose corresponding physical time period is $T = 2\pi(2ma_0^2/\hbar) = 3.0385 \times 10^{-16}$ sec. This very short oscillation period of the spin angular momentum can only be observed with a time resolution finer than 3.0385×10^{-16} sec. The experimental verification of this spin angular momentum perturbation will be the most remarkable discovery ever since the fundamental characteristics of the electron was proposed.

Preprints (www.preprints.org) | NOT PEER-REVIEWED | Posted: 19 July 2022 doi:10.20944/preprints202207.0284.v1

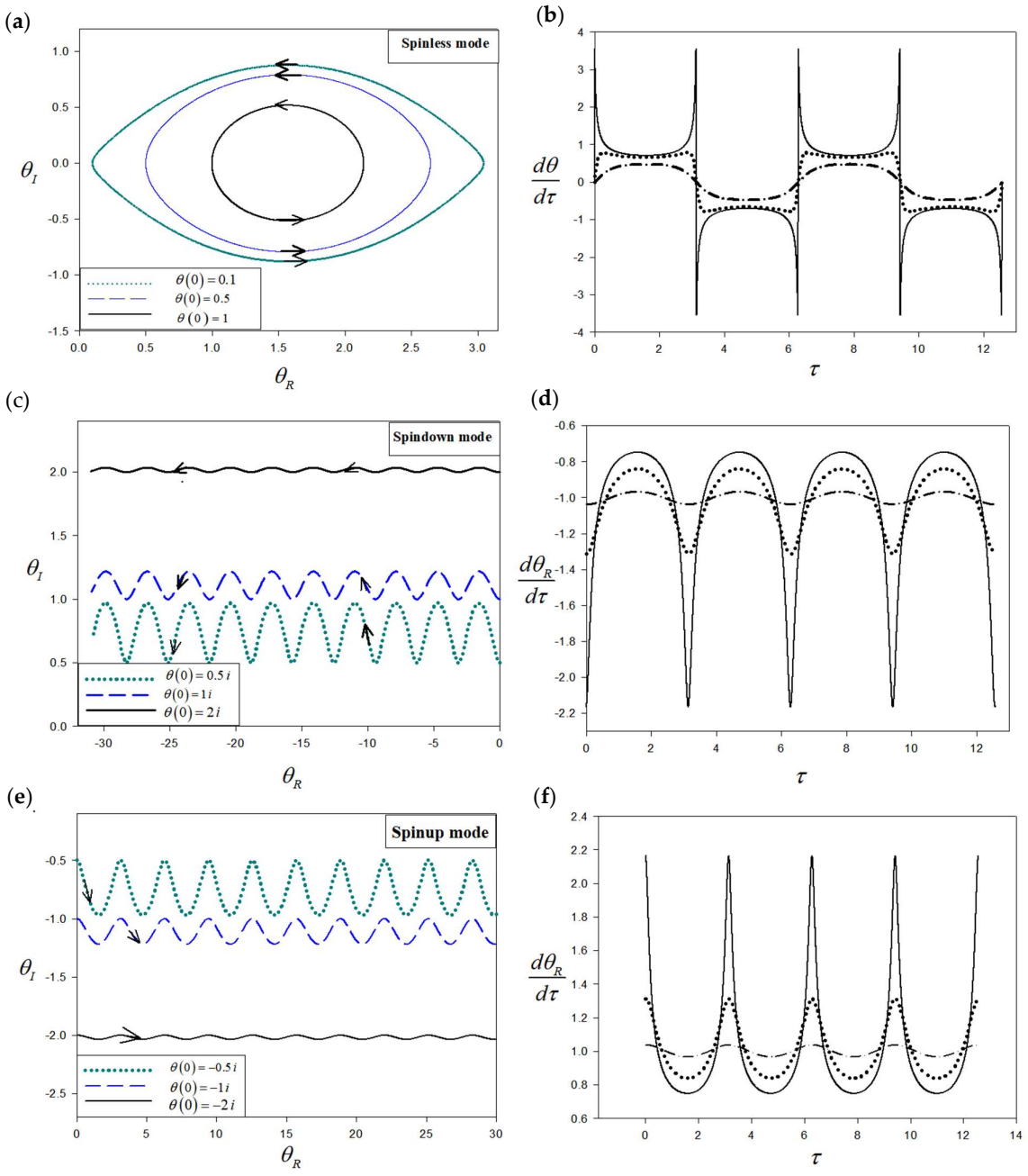

Figure 3. The three spin modes of the electron in the ground-state hydrogen atom: (**a**) The three spinless trajectories are demonstrated in the complex θ −plane at $\rho = 1$ with three initial conditions of θ: $\big(\theta_R(0), \theta_I(0)\big) = (0.1,0), (0.5,0)$, and $(1,0)$. (**b**) The time responses of $d\theta_R/d\tau$ of the three spinless trajectories are illustrated by the dashed-dotted line, dotted line, and solid line, showing zero mean angular velocity $\langle\dot{\theta}_R\rangle = 0$ in the spinless mode. (**c**) The three spin-down trajectories are demonstrated in the complex θ −plane at $\rho = 1$ with three initial conditions of θ: $\big(\theta_R(0), \theta_I(0)\big) = (0,0.5)$, $(0,1)$, and $(0,2)$; (**d**) The time responses of $d\theta_R/d\tau$ of the three spin-down trajectories are illustrated by solid-line, dotted line, and dashed-dotted line, showing mean angular velocity $\langle\dot{\theta}_R\rangle = -1$ in the spin-down mode. (**e**) The three spin-up trajectories are demonstrated in the complex θ −plane at $\rho = 1$ with three initial conditions: $\big(\theta_R(0), \theta_I(0)\big) = (0,-0.5)$, $(0,-1)$, and $(0,-2)$. (**f**) The time responses of $d\theta_R/d\tau$ of the three spin-up trajectories are illustrated by solid-line, dotted line, and dashed-dotted line, showing mean angular velocity $\langle\dot{\theta}_R\rangle = 1$ in the spin-up mode.

 doi:10.20944/preprints202207.0284.v1

3.2 Deriving Spin Dynamics from Schrödinger equation

In quantum mechanics, spin can only be revealed in the Dirac equation in which the relativity effect of the electron is considered. The reason that the spin dynamic cannot be exposed in the Schrödinger equation is the definition of the angular momentum in quantum mechanics, not because of the lack of consideration of the relativity effect. Let us inspect the expression of the angular momentum in complex space firstly. The quantum Hamiltonian (2.1) can be expressed in terms of the action function $S = -i\hbar \ln \psi$ as

$$H = \left[\frac{1}{2m}\left(\frac{\partial S}{\partial r}\right)^2 + \frac{\hbar}{2mi}\left(\frac{2}{r}\frac{\partial S}{\partial r} + \frac{\partial^2 S}{\partial r^2}\right)\right] + \frac{1}{2mr^2}\left[\left(\frac{\partial S}{\partial \theta}\right)^2 + \frac{\hbar}{i}\cot\theta\frac{\partial S}{\partial \theta} + \frac{\hbar}{i}\frac{\partial^2 S}{\partial \theta^2}\right] + \frac{1}{2mr^2\sin^2\theta}\left[\left(\frac{\partial S}{\partial \phi}\right)^2 + \frac{\hbar}{i}\frac{\partial^2 S}{\partial \phi^2}\right]. \quad (3.18)$$

The first bracket is only related to the radial motion, and we can express the remaining angular-related terms as:

$$L^2 = \left(\frac{\partial S}{\partial \theta}\right)^2 + \frac{\hbar}{i}\cot\theta\frac{\partial S}{\partial \theta} + \frac{\hbar}{i}\frac{\partial^2 S}{\partial \theta^2} + \frac{L_z^2}{\sin^2\theta}, \qquad L_z^2 = \left(\frac{\partial S}{\partial \phi}\right)^2 + \frac{\hbar}{i}\frac{\partial^2 S}{\partial \phi^2}, \quad (3.19)$$

where L can be identified as the orbital angular momentum and L_z is the $z-$component angular momentum in the complex domain. Using $S = -i\hbar \ln \psi$, it can be shown easily that L^2 and L_z are the functional representations of their corresponding quantum operators $\hat{L}^2$ and $\hat{L}_z$ as

$$\hat{L}^2\psi = L^2\psi, \quad \hat{L}_z\psi = L_z\psi \quad (3.20)$$

where

$$\hat{L}^2 = -\hbar^2\left(\frac{\partial^2}{\partial \theta^2} + \cot\theta\frac{\partial}{\partial \theta} + \frac{1}{\sin^2\theta}\frac{\partial^2}{\partial \phi^2}\right), \quad \hat{L}_z = \frac{\hbar}{i}\frac{\partial}{\partial \phi}. \quad (3.21)$$

The squared orbital angular momentum operator $\hat{L}^2$ gives rise to the quantization of the squared orbital angular momentum, which is described by the orbital quantum number $l(l+1)\hbar^2$. On the other hand, the quantization of $\hat{L}_z$ is described by the magnetic quantum number $m_l\hbar$. Let us consider the $2p$ state with $(n, l, m_l) = (2,1,1)$, as an example to show that L^2 and L_z can give exactly the same quantization result. Substituting the wave function ψ_{211} into Eq. (3.19), we have

$$L^2 = \frac{\hbar^2}{4}\left[(-3i\cot\theta)^2 + \left(\frac{\pm 2}{\sin\theta}\right)^2 + \cot^2\theta - 4(-\csc^2\theta)\right] = 2\hbar^2, \quad L_z = \hbar, \quad (3.22)$$

which is identical to the result given by the quantum numbers $l = 1$ and $m_l = 1$. The orbital angular momentum operator $\hat{L}^2$ roots from the convergence requirement of the Legendre polynomials. The admissible solutions ψ_{nlm_l} turn out to be the eigenfunctions of $\hat{L}^2$ with eigenvalues $l(l+1)\hbar^2$, i.e., $\hat{L}^2\psi_{nlm_l} = l(l+1)\hbar^2\psi_{nlm_l}$. This operator formulism is just the origin that excludes the spin angular momentum from $\hat{L}^2$. However, underlying the framework of QHM, we still can extract the spin angular momentum from L^2, the functional representation of $\hat{L}^2$.

The functional representation of $\hat{L}^2$ is given by Eq. (3.19), which can be rewritten with the help of Eq. (2.1) and Eq. (2.5) as

$$L^2 = \left[\left(mr^2\dot{\theta}\right)^2 + \left(mr^2\dot{\phi}\sin\theta\right)^2\right] + \left[\frac{\hbar^2}{4}\cot^2\theta - \hbar^2\left(\frac{\partial^2 \ln\psi}{\partial \theta^2} + \frac{1}{\sin^2\theta}\frac{\partial^2 \ln\psi}{\partial \phi^2}\right)\right], \quad (3.23)$$

in which the first bracket is the classical counterpart of the angular momentum and the second bracket is the quantum correction. When the electron is in the state with $l = m_l = 0$, we have $L^2 = 0$, $\dot{\phi} = 0$ and all the $\psi-$related terms are equal to zero. Then the remaining terms of Eq. (3.23) satisfy the following equation:

$$\left(mr^2\dot{\theta}\right)^2 = -\frac{\hbar^2}{4}\cot^2\theta. \quad (3.24)$$

The solution of the above equation reads

$$mr^2\dot{\theta} = \frac{\hbar}{2i}\cot\theta, \quad (3.25)$$

Preprints (www.preprints.org) | NOT PEER-REVIEWED | Posted: 19 July 2022 doi:10.20944/preprints202207.0284.v1

which is identical to Eq. (3.2), the spin angular momentum.

4. Dynamics of Electron's States Transitions

4.1 Energy Level Differences and Electric Field

The state transition problem is very similar to the orbit transfer problem in space engineering. The satellite needs the thrust to transfer from a lower-altitude orbit to a higher-altitude orbit. The required energy is needed to escape the gravitational attraction of Earth, which is analog to the transition energy that the electron needs to overcome the electrical attraction of the nucleus. However, there are two differences between two problems in different scales: (1) There is an additional force, the quantum force, acting on the electron; and (2) the states transition in hydrogen atom takes place in a complex space.

The time-dependent wave function describing the two-level energy transition is given by the superposition of the wave functions:

$$\Psi = C_1(t)\psi_1 e^{-iE_1 t} + C_2(t)\psi_2 e^{-iE_2 t}, \tag{4.1}$$

where the subscripts 1 and 2 stand for the initial state and the final state, respectively. The time-dependent coefficient $C_1(t)$ and $C_2(t)$ are determined by the Schrödinger equation with Ψ given by Eq. (4.1):

$$\frac{dC_1(t)}{dt} = -\frac{iV_{12}}{2\hbar} e^{-i(\omega_0-\omega)t} C_2(t), \tag{4.2a}$$

$$\frac{dC_2(t)}{dt} = -\frac{iV_{21}}{2\hbar} e^{i(\omega_0-\omega)t} C_1(t), \tag{4.2b}$$

where $V_{ij} = \int \psi_i^* V_{ext} \psi_j dz$ and $\omega_0 = (E_2 - E_1)/\hbar$. The external potential energy V_{ext} is provided by the electric field oscillating $z-$direction,

$$V_{ext} = -\frac{ezE}{2} e^{-i\omega}, \tag{4.3}$$

where E and ω represent the strength and frequncy of the electric field, respectively. The coefficients in Eq. (4.1) determine the occupation probability of the initial state and the final state,

$$P_1 = |C_1(t)|^2, \quad P_2 = |C_2(t)|^2, \tag{4.4}$$

which provides the quantum reference of the transition condition.

4.2 1s-2p State Transition

The 2p state $\psi_{210} = \rho e^{-\rho/2} \cos\theta$ has two shell structures as shown in Fig.4, and can be described by the total potential from Eq. (2.13):

$$\bar{V}_{Total} = \bar{V} + \bar{Q} = -\frac{2}{\rho} + \frac{1}{4\rho^2}(8 + cot^2\theta + 4sec^2\theta), \tag{4.5}$$

The equations of motion of the electron under the action of $\bar{V}_{Total}$ is given by Eqs. (2.15):

$$\frac{d\rho}{d\tau} = \frac{4-\rho}{i\rho}, \quad \frac{dz_\theta}{d\tau} = \frac{2-3z_\theta^2}{i\rho^2 z_\theta}, \quad \frac{d\phi}{d\tau} = 0. \tag{4.6}$$

The two shell structures can be distinguished by the equilibrium points, which are located at $\rho_{eq} = 4$ and $\theta_{eq} = cos^{-1}\left(\pm\sqrt{2/3}\right)$. Therefore, there are two spherical shells in the upper and lower real $x-y$ plane along the θ_{eq} direction, as the electron cloud exhibited in Fig. 4c. By solving Eq. (4.6), one can obtain the electron's trajectory in the 2p state. Fig. 5 displays the electron's trajectories starting from the initial positions $\big(\rho(0),\theta(0)\big) = (4,\pi/3) \in S_0$ and $\big(\rho(0),\theta(0)\big) = (4,\pi/3 \pm i) \in S_{\downarrow}(S_{\uparrow})$, which are illustrated by the solid-blue line and dashed-red line, respectively. It is clear to see that the electron with $\theta_I(0) = 0$ travels in a smaller region in the real $x-z$ plane; while the electron with $\theta_I(0) = \pm i$ contains the spin motion and travels farther than the one with no spin motion. It is the spin motion that makes the difference between the two trajectories. Fig. 5b illustrates the electron's motion in the complex $\theta-$plane. The closed trajectory circling the $\theta_{eq} = cos^{-1}\left(-\sqrt{2/3}\right)$ represents the spinless motion, and the open trajectories correspond to

Preprints (www.preprints.org) | NOT PEER-REVIEWED | Posted: 19 July 2022 doi:10.20944/preprints202207.0284.v1

spin down and spin up motion. The electron's spin motion has interaction with orbital motion in the 2p state , however, the basic feature of spinless and spin modes are still valid. The analysis of the interaction between orbital and spin dynamics refers to [59].

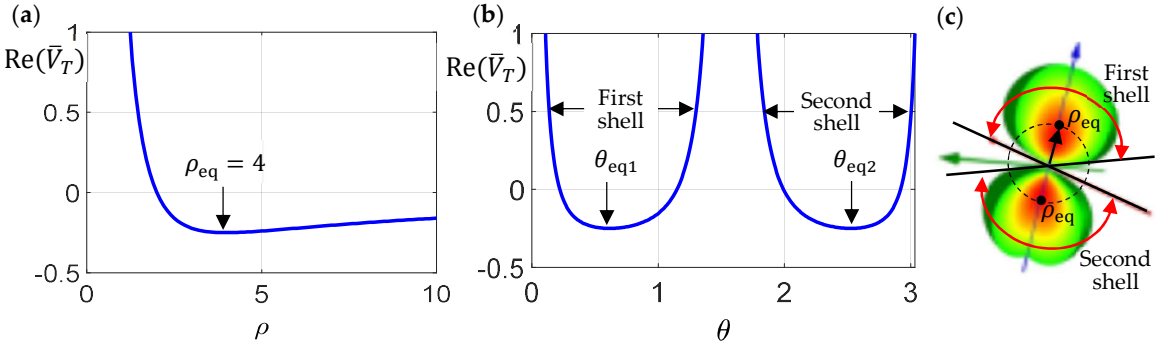

Figure 4. The variation of the real-part total potential of the 2p state: **(a)** in the radial direction with equilibrium position at $\rho_{eq} = 4$; **(b)** in the θ direction with equilibrium positions at $\theta_{eq} = cos^{-1}\left(\pm\sqrt{2/3}\right)$. **(c)** The probability distribution (electron cloud) of the 2p state has two shells along the θ direction and the brightest point locates at ρ_{eq} along the radial direction [58].

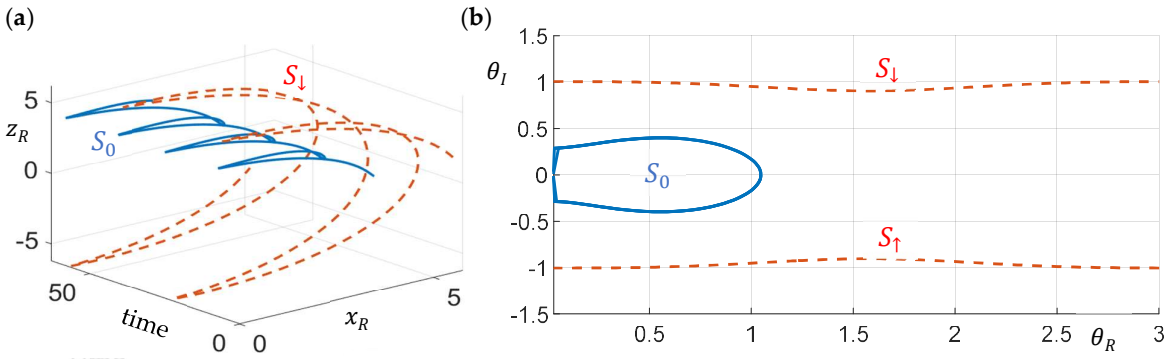

Figure 5. **(a)** The time evolution of the electron's complex trajectories of the 2p state in the real $x-z$ plane. The solid-blue line and dashed-red line represent the complex trajectories with initital positions $(\rho(0), \theta(0)) = (4, \pi/3) \in S_0$ and $(\rho(0), \theta(0)) = (4, \pi/3 \pm i) \in S_\downarrow(S_\uparrow)$, respectively; **(b)** The electron's trajectories in the complex θ −plane.

The wave function describes the 1s-2p state transition can be obtained according to Eq. (4.1),

$$\Psi = C_1(\tau)\psi_{100}e^{-i\bar{E}_1\tau} + C_2(\tau)\psi_{210}e^{-i\bar{E}_2\tau}, \tag{4.7}$$

where $\bar{E}_1 = -1$ and $\bar{E}_2 = -0.25$ are the energy levels of the 1s state and 2p state, respectively. By inserting ψ_{100} and ψ_{210} into Eq. (4.7), we have the following expression:

$$\Psi = C_1(\tau)e^{-\rho}e^{-i\bar{E}_1\tau} + C_2(\tau)\rho e^{-\rho/2}\cos\theta\, e^{-i\bar{E}_2\tau}, \tag{4.8}$$

in which the amplitude coefficients are determined by the following equations:

$$\dot{C}_1(\tau) = \rho(\tau)\cos\theta(\tau)\,\bar{E}e^{-i\Delta\bar{\omega}\tau}C_2(\tau)/2, \tag{4.9a}$$

$$\dot{C}_2(\tau) = \rho(\tau)\cos\theta(\tau)\,\bar{E}e^{i\Delta\bar{\omega}\tau}C_1(\tau)/2, \tag{4.9b}$$

where $\bar{\omega} = \omega_0 - \omega$. The state transition in hydrogen atom driven by electric field can be represented by the control block diagram as shown in Fig. 6, where the wave function (4.7) and the quantum dynamics (2.4) constitute the system model, and the applied electric field plays the role of the controller. The control procedures are stated as follows. (1) Iuput the time-dependent amplititude coefficients, $C_1(\tau)$ and $C_2(\tau)$, to the system model and the system model outputs the electron's transition trajectories, $\rho(\tau)$ and $\theta(\tau)$. (2) The system outputs are then measured by sensors and sent back to the controller as the feedback

Preprints (www.preprints.org) | NOT PEER-REVIEWED | Posted: 19 July 2022 doi:10.20944/preprints202207.0284.v1

signals. (3) The controller computes the error between the target state and the output state, and then adjusts the amplititude coefficients, $C_1(\tau)$ and $C_2(\tau)$, according to Eq. (4.9) based on the received feedback signals $\rho(\tau)$ and $\theta(\tau)$.

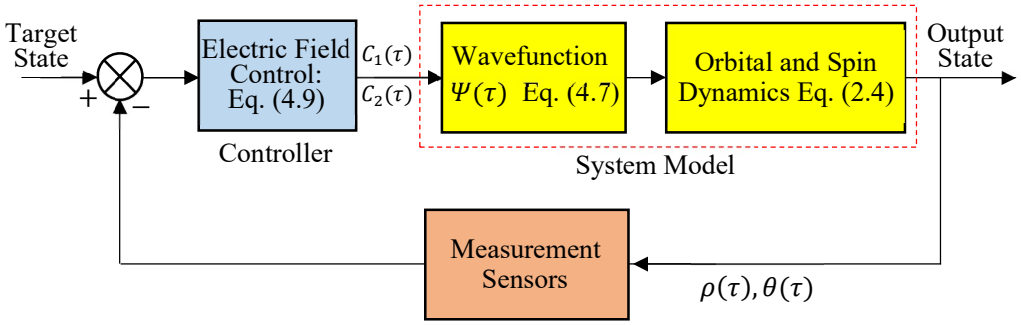

Figure 6. The control block-diagram representation of the two-level transition in hydrogen atom.

Next we will perform a computational simulation of the above control block diagram, where the electron is lauched at the initial position $(\rho(0), \theta(0)) = (4, \pi/3)$ in the 1s state and the transition to the target 2p state is driven by the electric field with strength $E = 8.8 \times 10^8\ V/m$ and frequncy $\omega = 1.548750\ 1/s$. The transition trajectory can be obtained by solving the equations of motion (2.4) with the wavefunction Ψ given by Eq. (4.7), and the result is illustrated in Fig. 7. The transition trajectory is observed to transit repeatedly between the 1s and 2p state, which is caused by the periodic change of the applied electric potential, as shown in Fig. 8a. The electron arrives at the 2p state when $P_1 = |C_1|^2 = 0$ and $P_2 = |C_2|^2 = 1$, at time $\tau = 1328$ (see Fig. 8c), where the electric field reaches its maximum value. After the electron reaches the farest point from the initial position, the applied electric field starts to decrease to its initial value and the electron returns to the 1s state when $P_1 = 1$ and $P_2 = 0$. In addition to the action of the eletric field, the electron's spin dynamics also participates in the transition process. From Fig. 7 we can see that the time response of θ_R is monotonically increasing or decreasing in the transition process and the same phenomenon can be observed in the spin dynamics as showm in Fig. 5a.

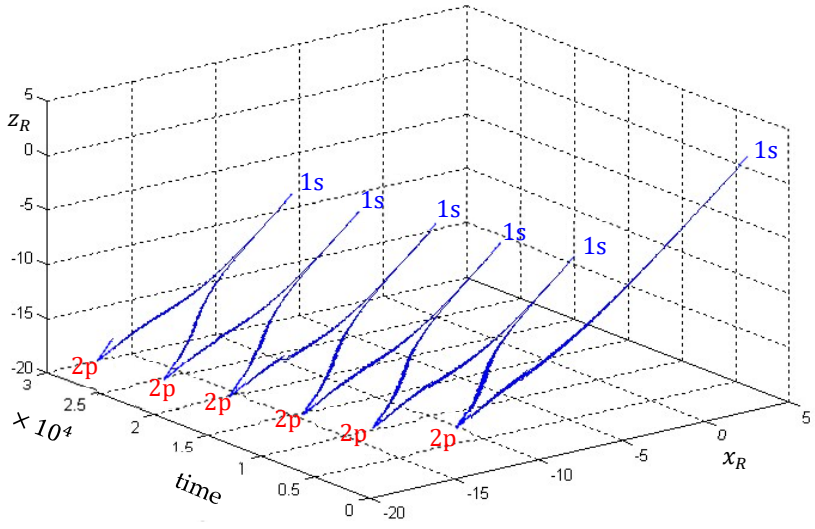

Figure 7. The time evolution of the 1s-2p transition trajectory in the real $x - z$ plane.

Preprints (www.preprints.org) | NOT PEER-REVIEWED | Posted: 19 July 2022 doi:10.20944/preprints202207.0284.v1

It is worthy to be noted that the maximum external electric potential $\bar{V}_{ext}$ is less than 0.05 (see Fig. 8a), but the energy gap between the 1s state and 2p state is $\Delta\bar{E} = \bar{E}_2 - \bar{E}_1 = -0.25 + 1 = 0.75$. How can the electron accomplish the transition with applied electric energy smaller than the energy gap? The answer lies in the quantum potential $\bar{Q}$. Let us has a closer insepection of the total energy in the transition,

$$\bar{E}_{Total} = \bar{V} + \bar{Q} + \bar{V}_{ext} + E_k. \tag{4.11}$$

as depicted in Fig. 8b. The quantum potential $\bar{Q}$ during the transition process can be expressed by

$$\bar{Q} = \frac{(4 + cot^2\theta)}{4\rho^2} + \frac{1}{4}\left[\frac{C_2\, cos\,\theta\left(C_1(\rho+4)e^{-i(\bar{E}_1+\bar{E}_2)\tau-\rho/2} - 4C_2\, cos\,\theta\, e^{-2i\bar{E}_2\tau}\right)}{2C_1C_2\rho\, cos\,\theta\, e^{-i(\bar{E}_1+\bar{E}_2)\tau-\rho/2} + \left(C_2\rho\, cos\,\theta\, e^{-i\bar{E}_2\tau}\right)^2 + C_1^2 e^{-2i\bar{E}_2\tau-\rho}}\right]$$
$$-\frac{1}{\rho^2}\left[\frac{C_2\rho\, cos\,\theta\, e^{-\rho/2}e^{-i\bar{E}_2\tau}}{C_1e^{-\rho}e^{-i\bar{E}_1\tau} + C_2\rho\, cos\,\theta\, e^{-\rho/2}e^{-i\bar{E}_2\tau}} + \frac{\left(C_2\rho\, sin\,\theta\, e^{-\rho}e^{-i\bar{E}_2\tau}\right)^2}{\left(C_1e^{-\rho}e^{-i\bar{E}_1\tau} + C_2\rho\, cos\,\theta\, e^{-\rho/2}e^{-i\bar{E}_2\tau}\right)^2}\right], \tag{4.12}$$

It can be seen from Fig. 8b that $\bar{E}_{Total}$ can change from its minimum value $\bar{E}_1 = -1$ at 1s state to its maximum value -0.25, with the range of change far beyond the magnitude of electric potential $\bar{V}_{ext} = 0.05$ (see Fig. 8a). Apparently, it is the quantum potential $\bar{Q}$ that complements the lack of the transition energy and provides the quantum force outwarding from the nucleus that leads the electron to reach the outside shell, the 2p shell. A similar quantum phenomenon happens in the tunneling process, where the particle's kinetic energy is found to be insufficient to overcome the potential barrier, and it is impossible from the viewpoint of classical mechanics to have the probability of finding the particle outside the potential barrier. However, the particle does appear outside the potential barrier. It is again the quantum potential that complement the required energy to the particle for overcoming the potential barrier. For more details on the classical interpretation of quantum effects by QHM, please refer to [60].

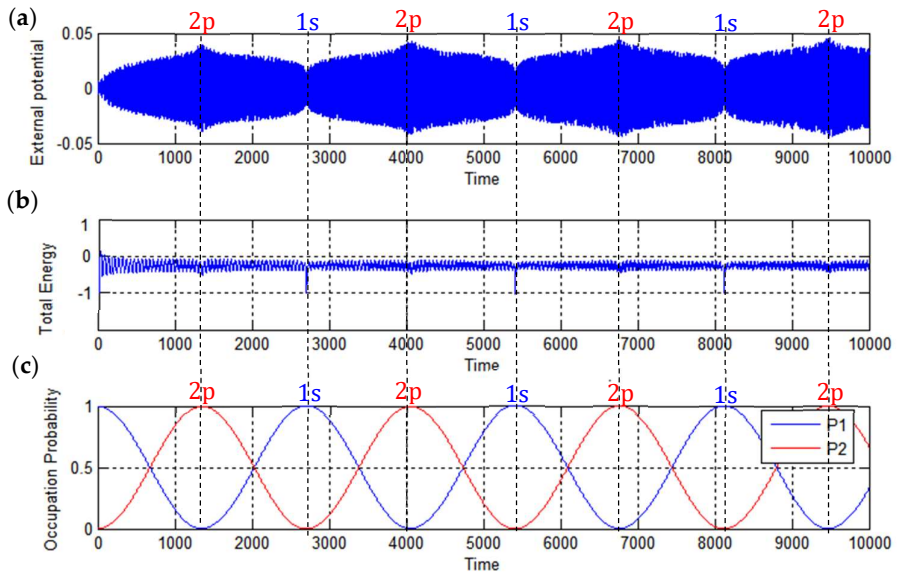

Figure 8. The time responses in the 1s-2p transition process: **(a)** The external electric potential energy $\bar{V}_{ext}(\tau)$; **(b)** The electron's total energy $\bar{E}_{Total}(\tau)$; **(c)** The occupation probabilities of the two states, $P_1(\tau) = |C_1|^2$, and $P_2(\tau) = |C_2|^2$.

5. Conclusions

The electron 1s-2p transition in the hydrogen atom driven by electric field is demonstrated. In the framework of QHM, the system model provides a perfect platform to analyze the electron's transition dynamics. Combining the orbital and spin dynamics together

in the model, the transition trajectory is oscillating between two states under the influence of the oscillating electric field. The electron's total energy varies between two eigen-energies with the same period as the transition trajectory. It shows that the electron has $\bar{E}_1 = -1$ at the 1s state and has the average energy of $\bar{E}_1 = -0.25$, when the 2p state is reached. The other interesting finding is that the electric potential energy in the transition process has the maximum value 0.04, which is much less than the energy difference $\Delta\bar{E} = \bar{E}_2 - \bar{E}_1 = -0.25 + 1 = 0.75$. It is the quantum potential that fills this energy gap and allows the electron to finish the transition.

The spin motion can only be revealed in the complex space as discussed in Section 3. When the orbital angular momentum is zero, the electron has an intrinsic spin angular momentum with values of $\pm\hbar/2$, which represent the spin up and spin down motions, respectively. An significant finding is that the electron's spin angular momentum is not a constant, but has a small periodic perturbation with period $T = 3.0385 \times 10^{-16}$ sec. It will be the remarkable finding of the electron's fundamental property if this small perturbation can be measured experimentally. According to the recent experiments of the electron spin [61,62], and the latest time precision improvement for the weak measurement to the order of 10^{-18} sec [63], we believe that the progress of detecting the spin properties will soon beyond the human's conventional knowledge about the spin.

Author Contributions: Conceptualization, C.-D.Y.; methodology, C.-D.Y.; software, S.-Y.H.; investigation, S.-Y.H.; writing—original draft preparation, S.-Y.H. All authors have read and agreed to the published version of the manuscript.

Conflicts of Interest: Declare conflicts of interest or state "The authors declare no conflict of interest."

References

1. Brion, E.; Molmer, K. Quantum computing with collective ensembles of multilevel systems. *Phys. Rev. Lett*. **2007**, *99*, 260501.
2. Li, W.P.; Yin, J.W.; Yu, Y.F.; Xiao, J.L.; Wang, Z.W. Quantum transition of two-level system in a parabolic quantum dot. *Int. J. Theor. Phys*. **2009**, *48*, 3339.
3. Yang, C.D.; Han, S.Y. Tunneling quantum dynamics in ammonia. *Int. J. Mol. Sci.* **2021**, *22,* 8282.
4. Han, H.S.; Lee, A.; Sinha, K.; Fatemi, F.K.; Rolston, S.L. Observation of vacuum-induced collective quantum beats. *Phys. Rev. Lett*. **2021**, *127*, 073604.
5. Lei, X.; Ma, L.; Yan, J.; Zhou, X.; Yan, Z.; Jia, X. Electromagnetically induced transparency quantum memory for non-classical states of light. *Adv. in. Phys.: X*. **2022**, *7*, 2060133.
6. Rao, J.; Li, B. Resonances of the hydrogen atom in strong parallel magnetic and electric fields. *Phys. Rev. A.* **1995**, *51*, 4526-4530.
7. Bartsch, T.; Main, J.; Wunner, G. The hydrogen atom in an electric field: closed-orbit theory with bifurcating orbits. *J. Phys. B: At. Mol. Opt. Phys.* **2003**, *36*, 1231-1254.
8. Tian, M.; Barber, Z.W.; Fischer, J.A.; Babbitt, W.R. Geometric manipulation of the quantum states of two-level atoms. *Phys. Rev. A.* **2004**, *69*, 050301.
9. Gao, J.; Daal, M.; Vayonakis, A. et al. Experimental evidence for a surface distribution of two-level systems in superconducting lithographed microwave resonators. *Appl. Phys. Lett*. **2008**, *92*, 152505.
10. Bowman, P.J. A "local observables" method for wave mechanics applied to atomic hydrogen. *Am. J. Phys.* **2008**, *76*, 1120-1129.
11. Messina, A.; Nakazato, H. Analytically solvable Hamiltonians for quantum two-level systems and their dynamics. *J. Phys. A: Math. Theor.* **2014**, *47*, 445302.
12. Lopez Carreno, J.C.; Sanchez Munoz, C.; del Valle, E.; Laussy, F.P. Excitation with quantum light. II. Exciting a two-level system. *Phys. Rev. A.* **2016**, *94*, 063826.
13. Oberreiter, L.; Burkhardt, J.; Main, J.; Wunner, G. Population transfer at exceptional points in the spectra of the hydrogen atom in parallel electric and magnetic fields. *Phys. Rev. A.* **2018**, *98*, 013417.
14. Sumner, I.; Anthony, H. Electron trajectories in molecular orbitals. *Int. J. Quantum. Chem.* **2020**, *120*, e26371.
15. Zheng, C. Quantum simulation of Pseudo-Hermitian-φ- symmetric two-level systems. *Entropy*. **2022**, *24*, 867
16. Holland; P. Uniqueness of paths in quantum mechanics. *Phys. Rev. A.* **1999**, *60*, 4326.
17. Colijn, C.; Vrscay, E.R. Spin-dependent Bohm trajectories for hydrogen eigenstates. *Phys. Lett. A.* **2002**, *300*, 334-340.
18. Colijn, C.; Vrscay, E.R. Spin-dependent Bohm trajectories associated with an electronic transition in hydrogen. *J. Phys. A: Math.Gen.* **2003**, *36*, 4689-4702.

19. Colijn, C.; Vrscay, E.R. Spin-dependent Bohm trajectories for Pauli and Dirac eigenstates of hydrogen. *Found. Phys. Letts.* **2003**, *36*, 303-323.
20. Colijn, C.; Vrscay, E.R. Quantum relaxation in hydrogen eigenstates and two-state transitions. *Phys. Lett. A*. **2004**, *327*, 113-122.
21. Shakov, Kh. Kh.; McGuire, J. H. Population control of 2s-2p transitions in hydrogen. *Phys. Rev. A.* **2003**, *67*, 033405.
22. Scheffler, T.B.; Malherbe, J.B. Complex energy eigenvalues of a zero-range atom in a uniform electric field. J. *Phys. A: Math. Gen.* **1979**, *12*, 1011-1023.
23. Farrelly, D.; Reinhardt, W.P. Uniform semiclassical and accurate quantum calculations of complex energy eigenvalues for the hydrogen atom in a uniform electric field. *J. Phys. B: Atom. Mol. Phys*. **1983**, *16*, 2103-2117.
24. Hertzberg, M.P.; Yamada, M. Vacuum decay in real time and imaginary time formalisms. *Phys. Rev. D*. **2019**, *100*, 016011.
25. Liu, C.S. The quantum phase transitions of dimer chain driven by an imaginary alternating field. *Physica E*. **2021**, *134*, 114871
26. Turro, F.; Roggero, A.; Amitrano, V.; Luchi, P.; Wendt, K.A.; Dubois, J.L.; Quaglioni, S.; Pederiva, F. Imaginary-time propagation on a quantum chip. *Phys. Rev. A.* **2022**, *105*, 022440.
27. Wang, M.S. Stochastic interpretation of quantum mechanics in complex space. *Phys. Rev. Lett.* **1997**, *79*, 3319-3322.
28. Kanatchikov, I.V. De Donder-Weyl theory and a hypercomplex extension of quantum mechanics to field theory. *Rep. Math. Phys.* **1998**, *42*, 157-170.
29. John, M.V. Modified de Broglie-Bohm approach to quantum mechanics. *Found. Phys. Lett.* **2002**, *15*, 329–343.
30. Schomerus, H. Topologically protected midgap states in complex photonic lattices. *Opt. Lett.* **2013**, *38*, 1912-1914.
31. Aharonov, Y.; Albert, D.Z.; Vaidman, L. How the result of a measurement of a component of a spin-1/2 particle can turn to be 100. Phys. *Rev. Lett.* **1988**. *60*, 1351-1354.
32. Aharonov, Y.; Botero, A. Quantum averages of weak values. *Phys. Rev. A*. **2005**, *72*, 052111.
33. Jozsa, R. Complex weak values in quantum measurement. *Phys. Rev. A*. **2007**, *76*, 044103.
34. Matzkin, A. Weak measurements of trajectories in quantum systems: classical, Bohmian and sum over paths. *J. Phys. A: Math. Theor*. **2015**, *48*, 305301.
35. Kocsis, S.; Braverman, B.; Ravets, S.; Stevens, M.J.; Mirin, R.P.; Shalm, L.K.; Steinberg, A.M. Observing the Average Trajectories of Single Photons in a Two-Slit Interferometer. *Science* **2011**, *332*, 1170–1173.
36. Murch, K.W.; Weber, S.J.; Macklin, C.; Siddiqi, I. Observing Single Quantum Trajectories of a Superconducting Quantum Bit. *Nature* **2013**, *502*, 211–214.
37. Zhou, Z.Q.; Liu, X.; Kedem, Y.; Cui, J.M.; Li, Z.F.; Hua, Y.L.; Li, C.F.; Guo, G.C. Experimental observation of anomalous trajectories of single photons. *Phys. Rev. A*. **2017**, *95*, 042121.
38. Procopio, L.M.; Rozema, L.A.; Wong, Z.J.; Hamel, D.R.; O'Brien, K.; Zhang, X.; Dakić, B.; Walther, P. Single-Photon Test of Hyper-Complex Quantum Theories Using a Metamaterial. *Nat. Commun*. **2017**, *8*, 15044.
39. Rossi, M.; Mason, D.; Chen, J.; Schliesser, A. Observing and verifying the quantum trajectory of a mechanical resonator. *Phys. Rev. Lett.* **2019**, *123*, 163601.
40. Ghafari, F.; Tischler, N.; Di Franco, C.; Thompson, J.; Gu, M.; Pryde, G.J. Interfering trajectories in experimental quantum-enhanced stochastic simulation. *Nat. Commun*, **2019**, *10*, 1630.
41. Naghiloo, M.; Tan, D.; Harrington, O.M.; Alonso, J.J.; Lutz, E.; Romito, A.; Murch, K.W. Heat and work along individual trajectories of a quantum bit. *Phys. Rev. Lett.* **2020**, *124*, 110604.
42. Karimi, B. Pekola, J.P. Quantum trajectory analysis of single microwave photon detection by nanocalorimetry. *Phy. Rev. Lett.* **2020**
43. Steinfurth, A. et al. Observation of photonic constant-intensity waves and induced transparency in tailored non-Hermitian lattices. *Sci. Adv.* **2022**, *8*, eabl7412.
44. Lee, T.E.; Chan, C.K. Heralded magnetism in non-Hermitian atomic systems. *Phys. Rev. X*. **2014**, *4*, 041001.
45. Helbig, T.; Hofmann, T. et. al. Generalized bulk-boundary correspondence in non-Hermitian topolectrical circuits. *Nat. Phys.* **2020**, *16*, 747-750.
46. Li, J.; Harter, A.K.; Liu, J. et. al. Observation of parity time symmetry breaking transitions in a dissipative floquent system of ultracold atoms, *Nature. Commun*. **2019**, *855*, 1.
47. Renou, M.O.; Trillo, D.; Weilenmann, M. et al. Quantum theory based on real number can be experimentally falsified. *Nature*. **2021**, *600*, 625-629.
48. Wu, K.D.; Kondra, T.V.; Rana, S.; Scandolo, C.M.; Xiang, G.Y.; Li, C.F.; Guo, G.C.; Streltsov, A. Resource theory of imaginarity: quantification and state conversion. *Phys. Rev. A.* **2021**, *103*, 032401.
49. Wu, K.D.; Kondra, T.V.; Rana, S. et al. Operational resource theory of imaginarity. *Phys. Rev. Lett.* **2021**, *126*, 090401.
50. Chen, M.C.; Wang, C.; Liu, F.M. et al. Ruling out real-valued standard formalism of quantum theory. *Phys. Rev. Lett.* **2022**, *128*, 040403.
51. Yang, C.D. Wave-particle duality in complex space. *Ann. Phys.* **2005**, *319*, 444-470.
52. Yang, C.D. Quantum Hamilton mechanics: Hamilton equations of quantum motion, origin of quantum operators, and proof of quantization axiom. *Ann. Phys.* **2006**, *321*, 2876-2926.
53. Yang, C.D. Trajectory interpretation of the uncertainty principle in 1D systems using complex Bohmian mechanics. *Phys. Lett. A.* **2008**, *372*, 6240-6253.
54. Yang, C.D.; Han, S.Y. Trajectory interpretation of correspondence principle: solution of nodal issue. *Found. Phys*. **2020**, *50*, 960–976.

 doi:10.20944/preprints202207.0284.v1

55. Yang, C.D.; Han, S.Y. Extending quantum probability from real axis to complex plane. *Entropy*, **2021**, *23*, 210.
56. Yang, C.D. Quantum dynamics of hydrogen atom. *Ann Phys*. **2005**, *319*, 399-443.
57. Yang, C.D. Complex spin and anti-spin dynamics: A generalization of de Broglie-Bohm theory to complex space. *Chaos, Soli & Frac.* **2009**, *41*, 317-333.
58. Herrmann, F.; Pohlig, M.; Avila, N.A. Simply atoms-atoms simply. *Lat. Am. J. Phys. Educ.* **2012**, *6*, 44-48.
59. Yang, C.D. Spin: nonlinear zero dynamics of orbital motion. *Chaos, Soli & Frac.* **2008**, *37*, 1158-1171.
60. Yang, C.D. Complex tunneling dynamics. *Chaos, Soli & Frac.* **2007**, *32*, 312-345.
61. Colangelo, G.; Ciurana, F.M.; Bianchet, L.C.; Sewell, R.J.; Mitchell, M.W. Simultaneous tracking of spin angle and amplitude beyond classical limits. *Nature*. **2017**, *543*, 525.
62. Cujia, K.S.; Boss, J.M.; Herb, K.; Zopes, J.; Degen, C.L. Tracking the precession of single nuclear spins by weak measurements. *Nature.* **2019**, *571*, 230.
63. Wang, Y.; Zhang, W.; Chen, S.; Wen, S.; Luo, H. Multiple-weak-value quantum measurement for precision estimation of time delay. *Phys. Rev. A.* **2022**, *105*, 033521.